J|A|C|S
ARTICLES
Published on Web 05/23/2006

cis,cis-$[(bpy)_2Ru^{V}O]_2O^{4+}$ Catalyzes Water Oxidation Formally via *in Situ* Generation of Radicaloid $Ru^{IV}-O\bullet$

Xiaofan Yang and Mu-Hyun Baik*

Contribution from the Department of Chemistry and School of Informatics, Indiana University, Bloomington, Indiana 47405

Received June 6, 2005; E-mail: mbaik@indiana.edu

Abstract: The mechanism of the catalytic oxidation of water by *cis,cis*-$[(bpy)_2Ru(OH_2)]_2O^{4+}$ to give molecular dioxygen was investigated using Density Functional Theory (DFT). A series of four oxidation and four deprotonation events generate the catalytically competent species *cis,cis*-$[(bpy)_2Ru^{V}O]_2O^{4+}$, which breaks the H−OH bond homolytically at the rate determining transition state to give a hydroperoxo intermediate. Our calculations predict a rate determining activation barrier of 25.9 kcal/mol in solution phase, which is in reasonable agreement with the previously reported experimental estimate of 18.7−23.3 kcal/mol. A number of plausible coupling schemes of the two metal sites including strong coupling, weak ferromagnetic and weak antiferromagnetic coupling have been considered. In addition, both high-spin and low-spin states at each of the Ru(V)-d^3 centers were explored and we found that the high-spin states play an important mechanistic role. Our calculations suggest that *cis,cis*-$[(bpy)_2Ru^{V}O]_2O^{4+}$ performs formally an intramolecular ligand-to-metal charge transfer when reacting with water to formally give a *cis,cis*-$[(bpy)_2Ru^{IV}O\bullet]_2O^{4+}$ complex. We propose that the key characteristic of the diruthenium catalyst that allows it to accomplish the most difficult first two oxidations of the overall four-electron redox reaction is directly associated with this *in situ* generation of two radicaloid oxo moieties that promote the water splitting reaction. A proton coupled metal-to-metal charge transfer follows to yield a Ru(V)/Ru(III) peroxo/aqua mixed valence complex, which performs the third redox reaction to give the superoxo/aqua complex. Finally, intersystem crossing to a ferromagnetically coupled Ru(IV)/Ru(III) superoxo/aqua species is predicted, which will then promote the last redox event to release triplet dioxygen as the final product. A number of key features of the computed mechanism are explored in detail to derive a conceptual understanding of the catalytic mechanism.

Introduction

The blue diruthenium complex *cis,cis*-$[(bpy)_2Ru(OH_2)]_2O^{4+}$ (bpy: 2,2′-bipyridine) is one[1−6] of very few structurally well-defined catalysts[7−13] competent of oxidizing water to yield molecular dioxygen at room temperature (eq 1). In green plants, a tetramanganese cluster found in the Oxygen Evolving

$$2\,H_2O \rightarrow O_2 + 4e^- + 4H^+ \qquad (1)$$

Complex (OEC) of photosystem II catalyzes this process.[14,15] The diruthenium catalyst provides a unique opportunity for understanding how two transition metal centers work in concert to oxidize water. Such atomic level understanding is important for rationally developing processes that may be utilized in artificial photosynthesis[16,17] and other critical future technologies. Despite intensive efforts in the past, no consensus mechanism exists to date, although a few plausible mechanisms have been proposed.[4,9] Detailed quantum chemical simulations of possible mechanistic scenarios addressing the energetic and electronic consequences of proposed reaction steps are desirable complements to traditional efforts. High-level quantum simulations of the diruthenium complex,[18,19] however, are challenging for many reasons. The necessity of modeling the bipyridine ligands explicitly and the transfer of four electrons and four protons add daunting complexity to the simulations. As the

(1) Gilbert, J. A.; Eggleston, D. S.; Murphy, W. R.; Geselowitz, D. A.; Gersten, S. W.; Hodgson, D. J.; Meyer, T. J. *J. Am. Chem. Soc.* **1985**, *107*, 3855−3864.
(2) Binstead, R. A.; Chronister, C. W.; Ni, J. F.; Hartshorn, C. M.; Meyer, T. J. *J. Am. Chem. Soc.* **2000**, *122*, 8464−8473.
(3) Chronister, C. W.; Binstead, R. A.; Ni, J. F.; Meyer, T. J. *Inorg. Chem.* **1997**, *36*, 3814−3815.
(4) Hurst, J. K. *Coord. Chem. Rev.* **2005**, *249*, 313−328.
(5) Hurst, J. K.; Zhou, J. Z.; Lei, Y. B. *Inorg. Chem.* **1992**, *31*, 1010−1017.
(6) Yamada, H.; Siems, W. F.; Koike, T.; Hurst, J. K. *J. Am. Chem. Soc.* **2004**, *126*, 9786−9795.
(7) Kitajima, N.; Osawa, M.; Tanaka, M.; Morooka, Y. *J. Am. Chem. Soc.* **1991**, *113*, 8952−8953.
(8) Sens, C.; Romero, I.; Rodriguez, M.; Llobet, A.; Parella, T.; Benet-Buchholz, J. *J. Am. Chem. Soc.* **2004**, *126*, 7798−7799.
(9) Rüttinger, W.; Dismukes, G. C. *Chem. Rev.* **1997**, *97*, 1−24.
(10) Naruta, Y.; Sasayama, M.; Sasaki, T. *Angew. Chem., Int. Ed. Engl.* **1994**, *33*, 1839−1841.
(11) Limburg, J.; Vrettos, J. S.; Liable-Sands, L. M.; Rheingold, A. L.; Crabtree, R. H.; Brudvig, G. W. *Science* **1999**, *283*, 1524−1527.
(12) Lei, Y. B.; Hurst, J. K. *Inorg. Chim. Acta* **1994**, *226*, 179−185.
(13) Lei, Y. B.; Hurst, J. K. *Inorg. Chem.* **1994**, *33*, 4460−4467.
(14) Yachandra, V. K.; Sauer, K.; Klein, M. P. *Chem. Rev.* **1996**, *96*, 2927−2950.
(15) Manchanda, R.; Brudvig, G. W.; Crabtree, R. H. *Coord. Chem. Rev.* **1995**, *144*, 1−38.
(16) Yagi, M.; Kaneko, M. *Chem. Rev.* **2001**, *101*, 21−35.
(17) Sun, L. C.; Hammarstrom, L.; Akermark, B.; Styring, S. *Chem. Soc. Rev.* **2001**, *30*, 36−49.
(18) Bartolotti, L. J.; Pedersen, L. G.; Meyer, T. J. *Int. J. Quantum Chem.* **2001**, *83*, 143−149.
(19) Yang, X.; Baik, M. H. *J. Am. Chem. Soc.* **2004**, *126*, 13222−13223.

10.1021/ja053710j CCC: $33.50

Scheme 1

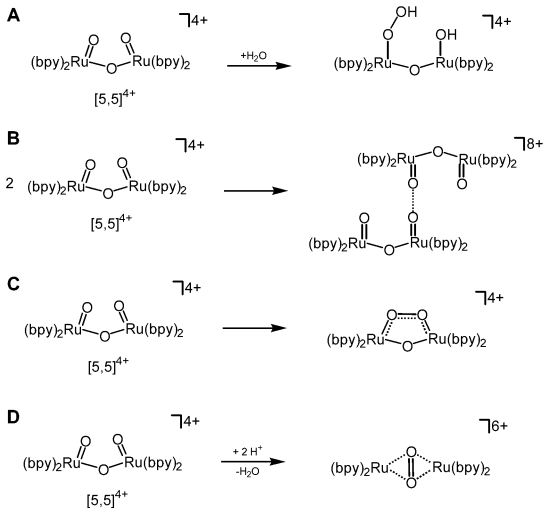

catalyst is highly reactive, key intermediates elude precise experimental detection giving rise to little definitive information that could be exploited for simplifying computer models and decreasing the size of the search space of structures and electronic configurations.

The ultimate goal of our work is to enable a more rational discourse on a fundamental level by providing details about the chemical and electronic nature of the intermediates and transition states of the catalytic mechanism that are currently neither identified nor conceptually understood.[4] There is general agreement that the catalytically competent diruthenium species is the $[(bpy)_2Ru^VO]_2O^{4+}$ ion. Scheme 1 highlights four possible mechanisms that have been considered in the past. Recent studies favor pathway A,[5] which invokes the formation of a hydroperoxo intermediate, while the alternative hypothesis, pathway B, implicating a "dimer of dimers"[20] is currently being questioned.[4] Other possibilities involve direct coupling of the terminal oxo groups and the formation of a familiar M_2O_2 "diamond core",[21−23] labeled as C and D, respectively. Although both are intuitively reasonable, they were ruled out in the past.[9] In exploratory studies, we surveyed both reaction paths A and B and found evidence for A being the most likely scenario. Therefore, we concentrated our efforts on reaction pathway A.

We present a computed reaction profile of one complete catalytic cycle addressing a few central questions: What is the nature of the rate-determining step and which electronic features are key to promoting that step? What is the role of the bridging ligand? How do the two redox-active metal centers work in concert? Is dioxygen formed directly or is the immediate product hydrogen peroxide, which rapidly converts to O_2? Answers to these and other questions are proposed. We were surprised to find a few disagreements between experiment and theory that could not be resolved. The most important discrepancies are described in some detail as challenges for future work, where both refinement of the computer simulation or reinterpretation of experimental results may be necessary.

Computational Details

All calculations were carried out using Density Functional Theory as implemented in the Jaguar 5.5 suite.[24] All geometries were optimized with the B3LYP[25−29] functional and the 6-31G** basis set. For Ru the Los Alamos LACVP basis[30,31] including relativistic effective core potentials was used. The energies of the optimized structures were reevaluated by additional single-point calculations using Dunning's correlation-consistent triple-ζ basis set[32] cc-pVTZ(-f). For Ru, we used a modified version of LACVP, designated as LACV3P, in which the exponents were decontracted to match the triple-ζ quality basis. Vibrational frequency calculations based on analytical second derivatives at the B3LYP/6-31G** (LACVP) level of theory were carried out on smaller models to derive the zero point vibrational energy (ZPVE) and entropy corrections at room temperature utilizing unscaled frequencies. By entropy, we refer specifically to the vibrational/rotational/translational entropy of the solute(s); the entropy of the solvent is implicitly included in the dielectric continuum model. The models for vibrational frequency calculations are obtained by replacing the bipyridine groups with ammonia ligands. Solvation energies were evaluated by a self-consistent reaction field (SCRF)[33−35] approach based on numerical solutions of the Poisson−Boltzmann equation.[36] These calculations were carried out at the optimized gas-phase geometries employing the dielectric constant of $\epsilon = 80.37$ (water). As is the case for all continuum models, the solvation energies are subject to empirical parameters for the atomic radii used to generate the solute surface. We employ the standard set[36] of radii for H (1.150 Å), C (1.900 Å), N (1.600 Å), O (1.600Å) and 1.481 Å for Ru. All calculations use the unrestricted spin formalism. Antiferromagnetic (AF) states were modeled using the broken symmetry (BS) orbital approach.[37,38] Manual adjustments to the initial guess functions were often necessary to converge to a plausible state, which was monitored by carefully observing Mulliken spin populations and visualizing the frontier molecular orbitals. When more than one stable structure was found, we compared the total energies and chose the structure with the lowest energy.

Results and Discussion

$[(bpy)_2Ru^{III}(OH_2)]_2O^{4+}$ − [3,3]$^{4+}$.[39] Whereas the structure of the procatalyst ion **[3,3]**$^{4+}$ is available,[1] its electronic structure is not fully understood. The two Ru(III)-d^5 centers are in pseudo-octahedral coordination geometry and are expected to display low-spin configuration, thus leaving one electron unpaired at each ruthenium site. EPR silence of **[3,3]**$^{4+}$ and magnetic susceptibility studies on the very analogous complex ion $[(bpy)_2(NO_2)Ru^{III}]_2O^{2+}$,[40] however, suggested a singlet ground state. Two possible electronic structure scenarios can be envisioned to explain this observation. First, the unpaired electrons from each metal site could couple strongly across the μ-oxo ligand

(20) Geselowitz, D.; Meyer, T. J. *Inorg. Chem.* **1990**, *29*, 3894−3896.
(21) Baik, M. H.; Newcomb, M.; Friesner, R. A.; Lippard, S. J. *Chem. Rev.* **2003**, *103*, 2385−2419.
(22) Lewis, E. A.; Tolman, W. B. *Chem. Rev.* **2004**, *104*, 1047−1076.
(23) Que, L.; Tolman, W. B. *Angew. Chem., Int. Ed. Engl.* **2002**, *41*, 1114−1137.
(24) Jaguar, *5.5 ed* Schrödinger, L. L. C, Portland, OR, 1991−2003.
(25) Becke, A. D. *Phys. Rev. A* **1988**, *38*, 3098−3100.
(26) Becke, A. D. *J. Chem. Phys.* **1993**, *98*, 5648−5652.
(27) Lee, C. T.; Yang, W. T.; Parr, R. G. *Phys. Rev. B* **1988**, *37*, 785−789.
(28) Slater, J. C. *Quantum Theory of Molecules and Solids, Vol. 4: The Self-Consistent Field for Molecules and Solids*; McGraw-Hill: New York, 1974.
(29) Vosko, S. H.; Wilk, L.; Nusair, M. *Can. J. Phys.* **1980**, *58*, 1200−1211.
(30) Hay, P. J.; Wadt, W. R. *J. Chem. Phys.* **1985**, *82*, 270−283.
(31) Hay, P. J.; Wadt, W. R. *J. Chem. Phys.* **1985**, *82*, 299−310.
(32) Dunning, T. H. *J. Chem. Phys.* **1989**, *90*, 1007−1023.
(33) Edinger, S. R.; Cortis, C.; Shenkin, P. S.; Friesner, R. A. *J. Phys. Chem. B* **1997**, *101*, 1190−1197.
(34) Cortis, C. M.; Friesner, R. A. *J. Comput. Chem.* **1997**, *18*, 1570−1590.
(35) Cortis, C. M.; Friesner, R. A. *J. Comput. Chem.* **1997**, *18*, 1591−1608.
(36) Rashin, A. A.; Honig, B. *J. Phys. Chem.* **1985**, *89*, 5588.
(37) Noodleman, L.; Lovell, T.; Han, W.-G.; Li, J.; Himo, F. *Chem. Rev.* **2004**, *104*, 459−508.
(38) Noodleman, L. *J. Chem. Phys.* **1981**, *74*, 5737−5743.
(39) The notation used throughout the study, e.g., [3, 3]$^{4+}$, denotes the oxidation states of each metal sites. These are formal assignments and are not intended to imply specific electronic structure patterns.
(40) Weaver, T. R.; Meyer, T. J.; Adeyemi, S. A.; Brown, G. M.; Eckberg, R. P.; Hatfield, W. E.; Johnson, E. C.; Murray, R. W.; Untereker, D. *J. Am. Chem. Soc.* **1975**, *97*, 3039−3048.

placing both electrons in the same MO to give a closed shell singlet state. Weak antiferromagnetic (AF) coupling that would leave the odd electron at each metal center unpaired and afford an open shell singlet state is a reasonable alternative. For 20 years, the former possibility was favored.[13,40,41] In our previous work,[19] we found that the AF coupling, approximated theoretically by use of the broken symmetry (BS) orbital approach,[37,38,42] is energetically preferable over the strongly coupled alternative. We showed that experimentally observed redox potentials of the diruthenium catalyst can only be reproduced computationally with the assumption of AF coupling. In principle, one additional electronic state must be considered, namely, the ferromagnetically (F) coupled triplet state. While the experimental evidence disfavors this possibility, we included it in our study for completeness and in part to obtain a reference state for estimating the 2*J*-coupling of the singlet state using Noodleman's spin projection techniques.[38,42] To our surprise, we found that the F-coupled state gives an even lower energy than the AF-coupled state. The computed energy difference between the F- and AF-coupled states is 4.1 kcal/mol in electronic energy *E*(SCF). Addition of zero point vibrational energies, entropies and solvation energies give a solution phase free energy difference of 5.7 kcal/mol. This finding constitutes a serious discrepancy between theory and experiment, as the experimental evidence suggests that the ferromagnetically coupled state is a few kcal/mol higher in energy than the AF-coupled state. The coupling constant 2*J* of the **[3,3]**$^{4+}$ ion has never been measured, but has been assumed to be close to -173 cm^{-1}, a 2*J* value determined for the related diruthenium complex $[(bpy)_2(NO_2)\text{-}Ru^{III}]_2O^{2+}$.[40] Thus, the BS state should be slightly lower in energy than the F-coupled state. We have exhaustively explored numerous possible electronic states of the BS state by enforcing different MO-occupation patterns and have examined all common exchange correlation functionals, in addition to varying the basis set, attempting to resolve this discrepancy, but have not been successful. A few of these efforts are mentioned in the Supporting Information. We concluded that the ferromagnetic and antiferromagnetic states of the **[3,3]**$^{4+}$ ion are close in energy and escape proper modeling by currently available methods. More precise and specific experimental data on the **[3,3]**$^{4+}$ ion might be helpful for refining the theoretical model.

For the present work, this discrepancy is tolerable, because we concentrate on the catalysis performed by the **[5,5]**$^{4+}$ ion (vide infra). As the **[3,3]**$^{4+}$ ion is the final product, it is clear that the computed overall driving force will likely be a few kcal/mol too low. As observed before in unrelated studies,[21] the geometry of the complex is not sensitive to the AF vs. F coupling scheme and, thus, we expect the computed structures of the **[3,3]**$^{4+}$ ion to be physically meaningful (Table 1). Compared to the experimental crystal structure, the computed bonds are slightly elongated with the Ru-μ-oxo bond being predicted to be 1.942 Å, which is 0.073 Å longer than the crystal structure data. One interesting question raised frequently in the past that could not be answered easily by experimental studies alone is whether there is structural flexibility around the O═Ru−O−Ru═O moiety. Our calculations show that the twisting motion of the molecule to yield what we label as the "eclipsed" conformer, denoting the notably smaller torsional angle θ(O2−Ru1−Ru2−O3) in Table 1, is energetically very viable with energy differences between the eclipsed and staggered geometries being 3.0 and 6.1 kcal/mol for the F- and AF-coupled complexes, respectively. Both structures are shown in Figure 1. Interestingly, this structural distortion leads to a notable bending of the Ru−O−Ru moiety to give an angle of 163°. As we will discuss below, the eclipsed arrangement of the terminal aqua/oxo ligands and the bending of the Ru−O−Ru moiety are intrinsically coupled and are crucial for promoting the water oxidation catalysis.

Table 1. Selected Bond Lengths (*r*) in Å, the Angle φ(Ru1−O1−Ru2) and the Torsional Angle θ(O2−Ru1−Ru2−O3) of the **[3,3]**$^{4+}$ Ion[a]

	staggered			
	exp.[1]	AF	F	S
r(Ru1−O1)	1.869	1.942	1.943	1.935
r(Ru2−O1)	1.869	1.942	1.942	1.931
r(Ru1−O2)	2.137	2.255	2.252	2.235
r(Ru2−O3)	2.137	2.254	2.250	2.265
φ(Ru1−O1−Ru2)	165.4	172.5	175.7	166.1
θ(O2−Ru1−Ru2−O3)	65.9	66.8	68.3	70.9
Δ*E*(SCF)	N/A	4.1	0.0	16.9
Δ*G*(Sol)	N/A	5.7	0.0	20.9

	eclipsed		
	AF	F	S
r(Ru1−O1)	1.941	1.934	1.919
r(Ru2−O1)	1.965	1.967	1.957
r(Ru1−O2)	2.222	2.223	2.206
r(Ru2−O3)	2.295	2.288	2.303
φ(Ru1−O1−Ru2)	163.1	163.3	152.3
θ(O2−Ru1−Ru2−O3)	26.5	28.5	20.5
Δ*E*(SCF)	3.6	−0.9	11.5
Δ*G*(Sol)	11.8	3.0	17.9

[a] Relative electronic energies and solution phase free energies are given in kcal/mol. The labels "staggered" and "eclipsed" refer to the two possible isomeric structures, illustrated in Figure 1.

$[(bpy)_2Ru^{V}O]_2O^{4+}$ − [5,5]$^{4+}$. A series of oxidation and deprotonation events ultimately give the complex **[5,5]**$^{4+}$, which is widely accepted to be the catalytically competent intermediate.[6,12] Because **[5,5]**$^{4+}$ is highly reactive, both its geometry and electronic structure have eluded precise detection thus far and will probably remain largely unresolved. Therefore, we have explored a number of possible structures and electronic configurations. Figure 2 and Tables 2 and 3 summarize the most important results. As seen for the **[3,3]**$^{4+}$ ion, two possible structural isomers and both AF and F coupling of the Ru(V)-d^3 centers were examined. The closed-shell singlet state is far too high in energy to be relevant.[19] Therefore, the closed-shell singlet state is not further discussed. Unlike in the case of **[3,3]**$^{4+}$, where only one reasonable configuration exists for the Ru(III)-d^5 core, both low-spin (LS) and high-spin (HS) states for the Ru(V)-d^3 center of the **[5,5]**$^{4+}$ ion can be envisioned, giving rise to one or three unpaired electrons at each of the ruthenium centers. These possibilities were also included in our study. Mulliken spin density analysis has proven to be an indispensable tool for monitoring the convergence to proper spin states in calculations involving complicated electronic structures.[21,43,44] For a low-spin AF-coupled Ru(V)-dimer one would

(41) Raven, S. J.; Meyer, T. J. *Inorg. Chem.* **1988**, *27*, 4478−4483.
(42) Lovell, T.; Han, W.-G.; Liu, T.; Noodleman, L. *J. Am. Chem. Soc.* **2002**, *124*, 5890−5894.
(43) Gherman, B. F.; Baik, M. H.; Lippard, S. J.; Friesner, R. A. *J. Am. Chem. Soc.* **2004**, *126*, 2978−2990.
(44) Baik, M.-H.; Gherman, B. F.; Friesner, R. A.; Lippard, S. J. *J. Am. Chem. Soc.* **2002**, *124*, 14608−14615.

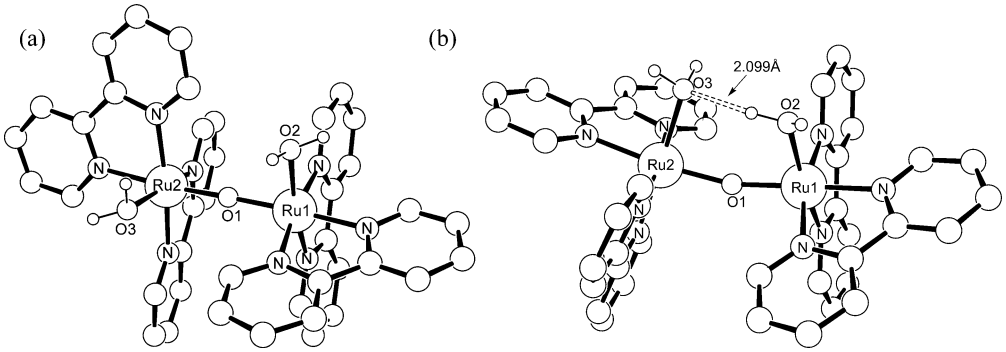

Figure 1. Two optimized structural isomers of **[3,3]**$^{4+}$ AF-coupled: (a) Staggered geometry. (b) Eclipsed geometry.

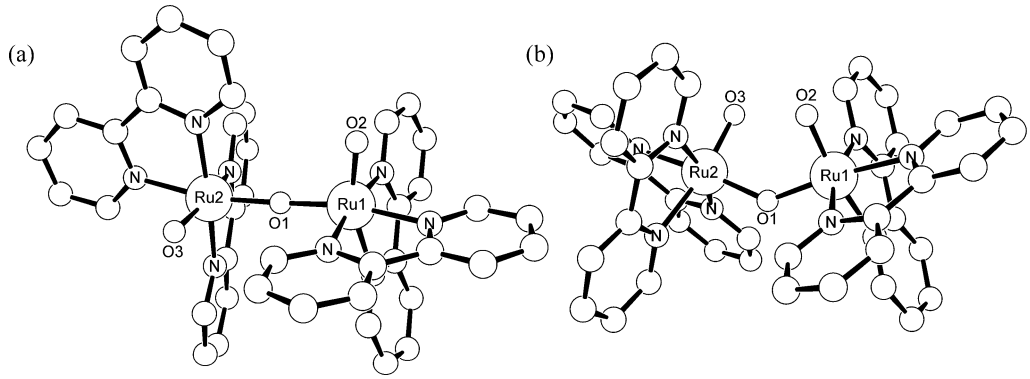

Figure 2. Two typical structural isomers of **[5,5]**$^{4+}$ AF-coupled: (a) Staggered geometry. (b) Eclipsed geometry.

Table 2. Selected Bond Lengths (r) in Å, the Angle φ(Ru1−O1−Ru2) and the Torsional Angle θ(O2−Ru1−Ru2−O3) of the **[5,5]**$^{4+}$ Ions[a]

staggered	F(HS)	F(LS)	AF(HS)	AF(LS)
r(Ru1−O1)	1.978	1.928	1.920	1.911
r(Ru2−O1)	1.977	1.929	1.918	1.910
r(Ru1−O2)	1.802	1.755	1.784	1.746
r(Ru2−O3)	1.801	1.755	1.785	1.747
φ(Ru1−O1−Ru2)	166.5	171.9	171.8	173.1
θ(O2−Ru1−Ru2−O3)	117.4	104.1	105.4	93.4
ΔE(SCF)	4.0	0.5	1.3	0.0
ΔG(sol)	8.1	2.8	3.6	0.0
$2J$			−210	−339
ΔE_0	4.5	1.0	1.8	0.0
eclipsed	**F(HS)**	**F(LS)**	**AF(HS)**	**AF(LS)**
r(Ru1−O1)	1.956	2.042	1.919	1.854
r(Ru2−O1)	1.957	1.889	1.919	2.106
r(Ru1−O2)	1.799	1.781	1.789	1.728
r(Ru2−O3)	1.799	1.721	1.790	1.780
φ(Ru1−O1−Ru2)	150.8	138.5	137.1	140.2
θ(O2−Ru1−Ru2−O3)	87.1	48.8	58.4	55.9
ΔE(SCF)	−2.3	11.9	0.4	6.1
ΔG(sol)	1.5	14.8	4.3	10.0
$2J$			N/A	−4065
ΔE_0	−1.8	12.4	0.9	6.6

[a] Relative electronic energies and solution phase free energies are in kcal/mol for **[5,5]**$^{4+}$ ion at different spin states. Heisenberg exchange coupling constants $2J$ are given in cm^{-1}. ΔE_0 is the spin-projected relative energies in kcal/mol.

Table 3. Mulliken Spin Densities

	Mulliken spin populations				
[5,5]$^{4+}$	Ru1	Ru2	O1	O2	O3
		staggered			
F(LS)	0.44	0.44	−0.62	0.88	0.89
F(HS)	1.39	1.38	0.92	1.11	1.11
AF(HS)	1.27	−1.27	0.00	1.00	−1.00
AF(LS)	0.59	−0.59	0.00	0.78	−0.78
		eclipsed			
F(LS)	0.41	−0.07	0.49	0.61	0.55
F(HS)	1.42	1.42	0.80	1.13	1.13
AF(HS)	1.48	−1.47	0.00	1.06	−1.06
AF(LS)	0.67	−0.74	0.50	0.57	−1.03

ideally expect spin populations of +1.0 and −1.0 on the two ruthenium centers, respectively, where the signs denote α and β spins. In reality, spin-delocalization on the ligands and the formalism of the Mulliken analysis give rise to notable reduction of the computed spin density from the expected ideal value. Typically, spin densities around 0.5 are seen for the low-spin Ru(V), whereas 2.5 can be considered typical for a high-spin Ru(V)-d^3 center. Table 3 lists spin densities that were used to monitor convergence to proper spin states. We have sampled dozens of electronic states for each of the possible configurations giving rise to a set of a few hundred species, which were all inspected using their spin densities, visualizations of their frontier MOs and total energies. Only the structures that we found to be chemically most meaningful are presented. Spin densities of the high-spin Ru(V) complexes are consistently and notably lower than expected, ranging from 1.27 to 1.48. We have carefully and extensively examined the electronic structure of these complexes and present an explanation for the seemingly too low spin density of the high-spin Ru(V) center below.

As observed for the **[3,3]**$^{4+}$ ion, the geometries are not very sensitive to the underlying electronic structure and comparable geometries were found for all four possible configurations, F(HS), F(LS), AF(HS) and AF(LS) states within the linear "staggered" and bent "eclipsed" geometries. In general, the structure of **[5,5]**$^{4+}$ is notably more compact than that of **[3,3]**$^{4+}$. At ∼1.7 Å the terminal Ru−O bonds are significantly shorter than the Ru−OH$_2$ bonds of **[3,3]**$^{4+}$ that were ∼2.3 Å. This

shortening is of course a direct indication of the increased Ru−O bond order from one to two. Interestingly, the Ru-μ-oxo distances are practically invariant at ∼1.9 Å, suggesting that the oxidation state changes of the ruthenium centers have little impact on the Ru−O−Ru bonding. Placing the terminal oxo groups in eclipsed conformation affects the Ru−O−Ru angle dramatically. Whereas only a moderate bending promoted by hydrogen bonding was found for the **[3,3]**$^{4+}$ ion to give Ru−O−Ru angles of ∼160° (Figure 1 and Table 1), it becomes significantly more acute at ∼140° in **[5,5]**$^{4+}$ (Figure 2 and Table 2).

The relative energies of the different electronic states are interesting. In general, the staggered geometry is favored with the lowest energy species being the *staggered*-AF(LS) complex. The AF-coupling is favored over F-coupling and we compute exchange coupling constants $2J$ of −339 and −210 cm^{-1}, respectively, for *staggered*-AF(LS) and the high-spin analogue *staggered*-AF(HS), which are reasonable values for systems of this type. Of mechanistic importance is the fact that the *eclipsed*-AF(HS) species is easily accessible with a free energy of 4.3 kcal/mol relative to the lowest energy species *staggered*-AF-(LS), whereas the *eclipsed*-AF(LS) shows a relative free energy of 10.0 kcal/mol. The *eclipsed*-AF(LS) state is also 5.8 kcal/mol lower in electronic energy (ΔE(SCF)) than the *eclipsed*-F(LS), giving rise to a nonrealistic exchange coupling constant of −4065 cm^{-1}. Inspection of the Ru1−O−Ru2 core structure of the *eclipsed*-AF/F(LS) states discloses the reason for this physically meaningless result. The concerted twisting and bending of the O═Ru−O−Ru═O moiety leads to a nonsymmetric distortion of the core, as indicated by Ru−O distances of 2.042/1.889 and 1.854/2.106 Å, respectively. After much experimentation, we concluded that both the F(LS) and AF(LS) states in eclipsed geometry are not constructive states for water oxidation, as they are energetically quite far away from the most favorable structure and show signs of structural instability that will ensue after the asymmetric structural distortion. Therefore, they are given in Table 2 only for completeness. We have also computed the spin-projected singlet state energies, which are expected to be lower than the BS-state energies. They are enumerated as ΔE_0 in Table 2. Consistent with the small exchange coupling, the spin-projection adds 0.5 kcal/mol to the BS-state energies. For simplicity, we use the uncorrected BS-state energies in this work.

The Mulliken spin density analysis (Table 3) exposes a key electronic feature of the **[5,5]**$^{4+}$ ion. The highly oxidizing ruthenium centers induce formally an intramolecular electron transfer event that moves electron density from the terminal oxo ligands to the metal centers, giving rise to a consistently lower spin density at the metal centers than intuitively expected. Although this effect can be observed for all isomers examined, as indicated by the development of significant radical character on O2 and O3 groups in Table 3, it is most pronounced in the high spin complexes. The spin densities on O2 and O3 in the *eclipsed*-AF(HS) of 1.06 and −1.06, respectively, indicate that electron densities equivalent to a full electron were transferred from the oxo groups to each of the ruthenium centers. As a result, the terminal oxo groups exhibit strong radicaloid character. One mechanistically helpful interpretation of this electronic structure is that the highly reactive **[5,5]**$^{4+}$ ion contains two •O−Ru(IV) units, instead of the formally correct O═Ru(V) moieties. Radicaloid oxygen centers are of course extremely powerful oxidants. The function of the metal center in this conceptual model is the *in situ* generation of an oxyl radical that ultimately performs the oxidative water splitting reaction. We proposed a similar concept previously in a different, unrelated context for the C−H activation catalysis performed by an $Fe^{IV}_2O_2$ core structure found in soluble *methane monooxygenase*.[44] It is easy to understand why this effect is strongest in high spin AF-coupled configurations, as both high-spin configuration and AF-coupling give rise to lower energy frontier orbitals in the d-orbital manifold and, thus, should generate the strongest driving force for accepting an electron.[45]

Redox Potentials. Comparing calculated results with experimentally observable properties is important for establishing the credibility of the computer model. In the present case, where the redox properties of the catalyst play a key role, redox potentials provide a convenient and appropriate reference for benchmarking the computer model. Previously, we demonstrated that a series of experimentally observed redox potentials can be reproduced within ∼100 mV assuming AF-coupling,[19] except for the redox process shown in eq 2. Our calculations gave a

$$\mathbf{[5,5]}^{4+} + e^- \rightarrow \mathbf{[4,5]}^{3+} \qquad E_{1/2}(\text{exp.}) = 1.40 \text{ V vs. NHE}^2 \quad (2)$$

redox potential of 1.887 V vs. NHE for this redox reaction. The unusually large deviation of 0.487 V from the experimentally measured potential of 1.40 V casts doubt about the correctness of the computed electronic structure. This inconsistency is serious, as it involves the **[5,5]**$^{4+}$ ion that serves as the starting point of our mechanistic investigation.[46] Thus, we examined the electronic structure of the **[5,5]**$^{4+}$ ion in great detail and searched for possible isomers with lower energies, without being able to detect alternative structures that correlate better with the experimentally observed redox potentials. Given that the redox potentials were measured in acidic media,[2] where electron and proton transfers are often coupled, we also considered the possibility that the experimentally observed redox reaction includes a proton transfer and recomputed the redox

$$\mathbf{[5,5]}^{4+} + e^- + H^+ \rightarrow \mathbf{[4,5]}^{4+} \qquad E_{1/2}(\text{calc.}) = 1.429 \text{ V vs. NHE} \quad (3)$$

potential assuming the involvement of a proton (eq 3). Our calculated potential of 1.429 V for the **[5,5]**$^{4+}$/**[4,5]**$^{4+}$ redox pair is in good agreement with the experimentally observed potential of 1.40 V vs. NHE.[47] This result suggests that the previously observed redox event at 1.40 V is a proton-coupled redox event as shown in eq 3. We note that the thermodynamic stability of **[4,5]**$^{x+}$ has been questioned in the past.[48] Our calculations suggest that if **[4,5]**$^{x+}$ is assumed to be stable, the redox event at 1.40 V must be proton coupled. The fact that the potential was pH independent may be interpreted as evidence that **[4,5]**$^{x+}$ is not stable, as suggested before, and a different redox reaction takes place at 1.40 V. Further studies are being carried out to delineate this conflicting issue.

(45) Baik, M.-H.; Lee, D.; Friesner, R. A.; Lippard, S. J. *Isr. J. Chem.* **2001**, *41*, 173−186.
(46) We thank one reviewer for helpful comments on this critical issue.
(47) See Supporting Information for details.
(48) Yamada, H.; Hurst, J. K. *J. Am. Chem. Soc.* **2000**, *122*, 5303−5311.

Scheme 2

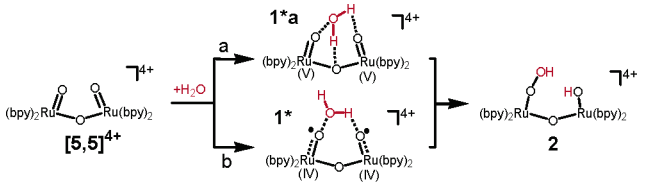

Formation of the Reactant Complex 1*. The mechanistic proposal involving an initial attack of the **[5,5]**$^{4+}$ ion by a solvent water molecule has received much support recently.[4,6] Our calculations support this concept and reveal that initial attack by a solvent water molecule is very reasonable both energetically and electronically. At the beginning of this catalytic cycle stands the formation of a reactant complex between the **[5,5]**$^{4+}$ ion, **1**, and a solvent water molecule to give complex **1***. The exact structure of this precursor complex has been speculated upon in the past.[5] The formation of the precursor complex is important for understanding the subsequent reaction step yielding the peroxo intermediate, as shown in Scheme 2. This step is crucial, because it accomplishes a substantial portion of the overall reaction, i.e., the transfer of two electrons and the formation of the O−O bond.

A key issue that must be addressed is how and why the oxygen atom of the water molecule is attracted to a terminal oxo group of the catalyst. Previously, the concert of two hydrogen bonds was suggested to connect the water molecule simultaneously to the μ-oxo ligand and to one of the terminal oxo groups. This structural arrangement, labeled as **1*a** in Scheme 2, offers an intuitive rationalization for the mechanistically required alignment of the oxygen atom in water with one of the terminal oxo groups in the catalyst. We probed specifically for **1*a** and found no evidence for the thermodynamic stability of such complex. For the μ-oxo moiety to serve as a hydrogen-bond acceptor, a substantial structural distortion is required, which is sterically and electronically not viable. Instead, we found that there is an intrinsic attraction between the terminal oxo group of the catalyst and the oxygen atom of water, as the radicaloid oxyl moiety of the catalyst attacks water in an electrophilic fashion. The proposed reactant complex is shown in Scheme 2 as **1*** and the computed structure is presented in Figure 3. The oxygen−oxygen interaction is weak at a distance of 3.420 Å (Figure 4) and although we show a dotted line between the water-H and O2 for illustrative purposes, there is no hydrogen bonding between water and the terminal oxo group

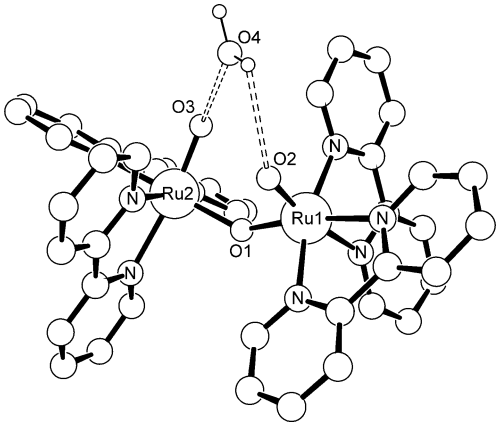

Figure 3. Optimized structure of the reactant complex **1***.

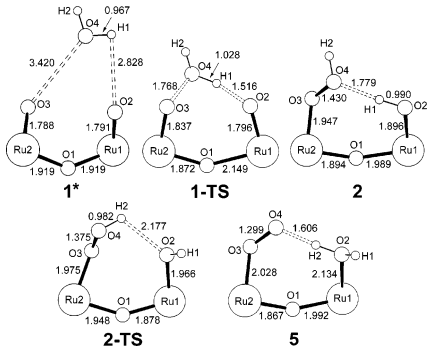

Figure 4. Selected core structure changes during catalytic cycle. Bond lengths are given in Å.

Table 4. Mulliken Spin Densities

	Ru1	Ru2	O1	O2	O3	O4
1*	1.46	−1.46	0.01	1.07	−1.08	0.00
1-TS	1.09	−1.19	−0.71	0.83	−0.14	0.15
2	1.21	−1.05	−0.28	0.39	−0.25	−0.04
2-TS	1.29	−1.04	0.16	0.18	−0.43	0.16
5	0.71	−1.20	−0.50	0.01	0.44	0.54
5′	0.89	0.67	0.77	0.00	0.75	0.89
6	0.31	−0.29	−0.02	0.00	0.00	0.00
6′	0.63	0.59	0.79	0.00	1.04	0.95
7	0.32	−0.32	0.00	0.00	0.00	0.00

in the reactant complex **1*** at a distance of 2.828 Å. Spin densities of ±1.46 at Ru and ±1.07 at the terminal oxo ligands (Table 4) indicate that there is only a small electronic perturbation by the weak attachment of water to the eclipsed AF(HS)-**[5,5]**$^{4+}$ ion. Without the additional water ligand, spin densities of ±1.48 at Ru and ±1.06 at the terminal oxo groups were found.

Catalytic Mechanism. Scheme 3 and Figures 4 and 5 summarize the calculated mechanism starting from the reactant **1**, the low-spin AF-coupled **[5,5]**$^{4+}$ ion in the most relaxed staggered geometry, and a free water molecule,[49] which serve as the reference for all relative energies. The most important frontier orbitals are t_{2g}-like orbitals in the pseudo-octahedral ligand environment and are therefore labeled as such for simplicity. The electronic structure of the diruthenium core that is most consistent with the Mulliken spin density analysis and a more detailed MO-analysis is summarized in Scheme 3. The formation of **1***, modeled here by adding one explicit water molecule to **1**, is an endothermic process with a relative energy of 20.2 kcal/mol, where two chemical processes occur. First, **1*** is in eclipsed geometry and is the high-spin AF-coupled complex, where the intramolecular electron transfer to give the oxyl-radical moiety described above has taken place. Second, a water molecule is attached to the complex without being activated. This free energy difference is of course mostly due to entropy loss. The energy components are enumerated in greater detail in the Supporting Information.

It is important to realize that while addition of one water is required for constructing a mass-balanced reaction energy profile, the energy of the complex is likely not reliable. In principle, the *eclipsed*-AF(HS) complex and **1*** should be isoenergetic subject to accounting for the free energy of one

(49) Entropy and solvation corrections for the free water molecule have of course been added consistently. See Supporting Information for all energy components.

Scheme 3

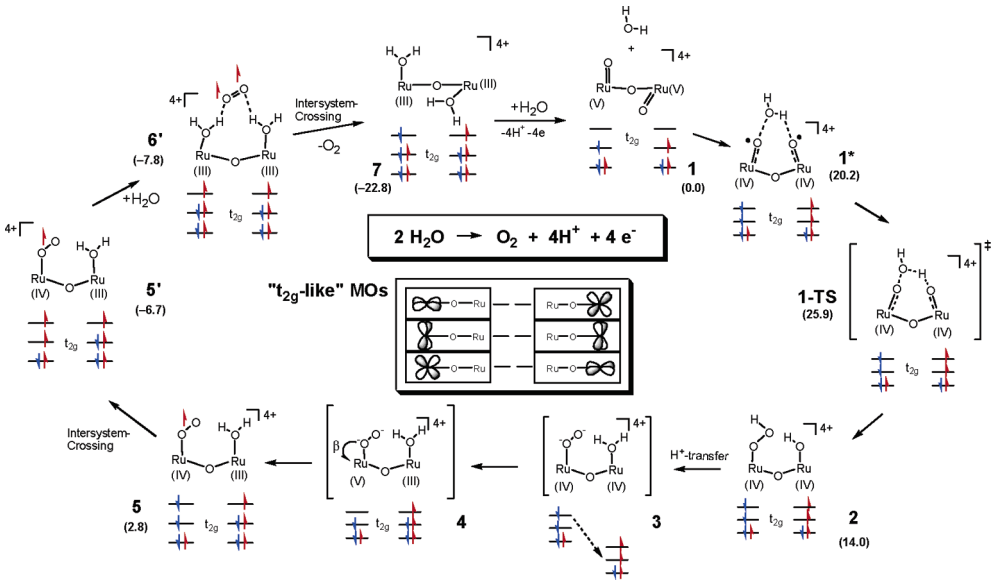

explicit water, since the additional water molecule is simply one of the first shell solvent molecules. Formally, species **1*** can therefore be considered a model of the *eclipsed*-AF(HS) complex where the continuum solvation model has been mixed with a partial, explicit solvent model. Species **1***, however, is 15.9 kcal/mol higher in energy than the sum of the *eclipsed*-AF(HS) complex and one solvated water molecule, demonstrating that mixing explicit and continuum solvation model is problematic.[50] This is a general problem of modeling solvation that can be reproduced in any continuum solvation treatment of reactions, but are particularly prominent in reactions where solvent molecules become reactants. The reason lies in the fact that representing a solute−solvent cluster that is highly dynamic in character with only one solvent in a static geometry is inappropriate. To obtain a more reliable model, a large number of possible structures must be explored adding increasingly more solvent molecules and equilibrating their structures until the total energy converges.[51] Ideally, the real energy must be determined as the weighted ensemble average of a statistically meaningful number of solvent−solute clusters. Adding one solvent molecule in an *ad hoc* fashion introduces noncanceling errors that are not likely to improve the continuum treatment of solvation. Since the energy of **1*** has no mechanistically relevant meaning, we treat it as a transient intermediate recognizing that our computed energy for **1*** is not meaningful.

The first step of the catalysis involves the cleavage of the H−OH bond and formation of a RuO−OH bond from the reactant complex **1*** to yield the hydroperoxo intermediate **2**. As highlighted in Figure 5, this transformation is rate determining with a computed solution phase free energy of activation of 25.9 kcal/mol, measured as the energy difference between **1-TS** and **1**. This value is reasonable for a reaction that completes readily at room temperature, and is in good agreement with experimental estimates of 18.7−23.3 kcal/mol.[6] Intermediate **2** rapidly undergoes a series of electronic transformations initiated by a transfer of the hydroperoxo-proton to the hydroxyl group, formally yielding the peroxo-aqua complex **3**. We show this complex for conceptual understanding in Scheme 3, but species **3** is not stable and cannot be located on the potential energy surface as a true intermediate. As a result of the proton transfer, one ruthenium center carries a neutral aqua ligand, whereas a dianionic peroxo ligand is attached to the other ruthenium center. This heterogeneous ligand environment is no longer able to support a symmetric Ru(IV)/Ru(IV) configuration. Formally, a disproportionation event follows to yield the Ru(III)/Ru(V)-aqua/peroxo complex **4**, where a highly oxidizing Ru(V) center is placed next to the electron-rich peroxo ligand.

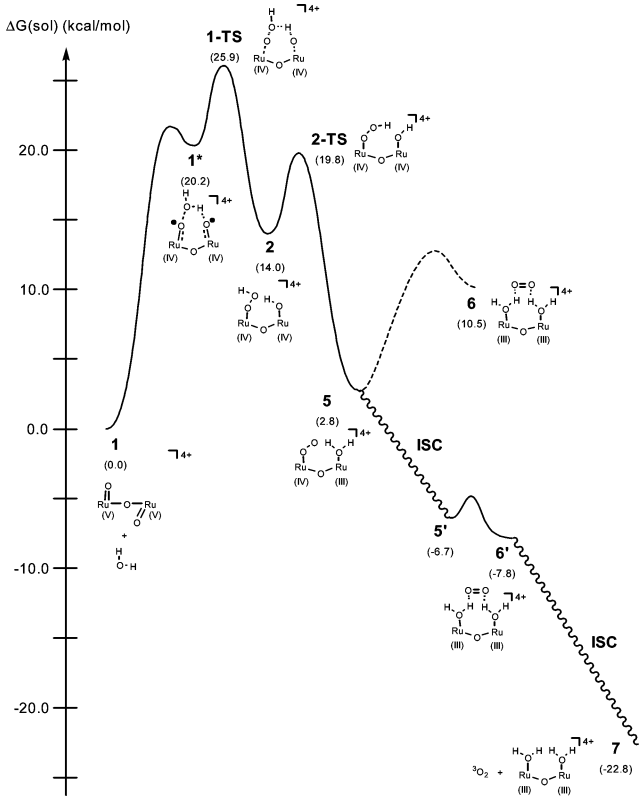

Figure 5. Computed catalytic mechanism of water oxidation.

(50) Baik, M. H.; Friesner, R. A.; Lippard, S. J. *J. Am. Chem. Soc.* **2002**, *124*, 4495−4503.
(51) Tawa, G. J.; Topol, I. A.; Burt, S. K.; Caldwell, R. A.; Rashin, A. A. *J. Chem. Phys.* **1998**, *109*, 4852−4863.

Of course, spontaneous intramolecular oxidation follows to give the Ru(III)/Ru(IV)-aqua/superoxo species **5** at a relative energy of $\Delta G(\mathrm{sol}) = 2.8$ kcal/mol. Our spin density analysis indicates clearly that the peroxo group donates a β-spin electron, giving rise to an α-electron radical that is delocalized on the two oxygen atoms of the newly formed superoxo group in **5**. O3 and O4 show spin densities of 0.44 and 0.54, respectively (Table 4), whereas densities of 0.71 and −1.20 on Ru1 and Ru2 identify Ru(III) and Ru(IV), as illustrated in Scheme 3. In summary, the intimate coupling of proton shift, disproportionation and ligand to metal electron-transfer accomplished the transfer of a β-electron from O2 across the μ-oxo bridge to Ru2. We were able to locate a transition state for this complicated process, labeled as **2-TS** in Figure 5. The core structure of this transition state is given in Figure 4. Structurally, **2-TS** is characterized by loss of a hydrogen bond between O4 and H1 in **2**, which is a very strong interaction at a distance of 1.779 Å, to afford a weak hydrogen bond between H2 and O2 after rotation of the hydroperoxo moiety. Although the Ru2−O1 and O1−Ru1 bonds also change notably by 0.054 and −0.111 Å, respectively, the spin densities of −1.04 and 1.29 at Ru2 and Ru1, respectively, indicate that the above-described metal−metal charge transfer has not yet taken place at the transition state. The O4−H2 bond distance of 0.982 Å is additional evidence for an early transition state that is energetically, structurally and electronically close to intermediate **2**. The driving force for this rapid conversion step **2** → **5** accomplishing the third oxidation event is 11.2 kcal/mol.

The Ru(IV) site in **5** is poised to accept an α-electron, as illustrated in the schematic MO-diagram of **5** in Scheme 3. The superoxo moiety is an α-radical in **5** indicated by α-spin densities of 0.44 and 0.54 on O3 and O4, respectively. Therefore, the most natural course of action is to transfer the unpaired α-electron from the superoxo ligand to Ru2(IV) and generate the product complex **6**, consisting of a singlet molecular dioxygen and an AF-coupled Ru(III)/Ru(III) complex. Interestingly, our calculations suggest that this last oxidation step is highly unfavorable thermodynamically. The singlet dioxygen-diruthenium complex **6** is 7.7 kcal/mol higher in energy (Figure 5) than intermediate **5**. The dioxygen formed in this product complex was considered to be in the $^1\Delta_g$ state. Since the $^3\Sigma_g$ state of dioxygen is expected to be ∼22 kcal/mol lower in energy than the $^1\Delta_g$ state, we considered an alternative path that would give access to triplet dioxygen, which requires intersystem crossing (ISC). We showed previously that dimeric transition metal systems are particularly effective in promoting ISC.[43] Starting from **5**, the unpaired electron of the Ru(IV) site is first inverted to give the ferromagnetically coupled analogue **5′**, a quintet state, which is 9.4 kcal/mol lower in energy than **5**. Although it is currently impossible to determine the efficiency of ISC events in complex molecules of this type, the thermodynamic driving force for the **5** → **5′** transformation makes such an event reasonable. The Ru(IV) center in **5′** can easily accept one β-electron from the superoxo moiety yielding the quintet complex **6′** after addition of one water molecule, where the two Ru(III)-d^5 centers are ferromagnetically coupled. This reaction is 1.1 kcal/mol downhill from the superoxo intermediate **5′**. Release of triplet dioxygen and another intersystem crossing recovers the initial AF-coupled **[3,3]**$^{4+}$ complex, labeled as **7** in Scheme 3 and Figure 5.

Two features of the catalytic cycle are mechanistically significant: First, we propose that the immediate product of the oxidation mechanism is molecular dioxygen and not hydrogen peroxide. The hydroperoxo complex **2** is separated from the superoxo complex **5** only by a barrier of 5.8 kcal/mol. Thus, we predict a rapid conversion of hydroperoxo complex to the higher oxidized species. Possible ligand displacement reactions involving water to generate hydrogen peroxide as the final product are likely not competitive. Second, our simulation predicts the release of triplet rather than singlet dioxygen. So far, no experimental work has been reported on this issue. As the spin state of the released dioxygen should be accessible to spectroscopic detection, we put forth this theoretical prediction as a challenge for future experimental testing. Depending on the efficiency of the ISC-conversion **6′** → **7**, which is potentially not very high, the paramagnetic, F-coupled species **6′** may display a lifetime that makes this transient intermediate spectroscopically detectable.

Electron Trafficking Across the μ-oxo Ligand. The proposed mechanism invokes an intramolecular electron transfer across the μ-oxo bridge as a key step that we illustrate by formally considering the hypothetical transient intermediate **3** in Scheme 3. The hydroperoxo moiety has direct access to only one ruthenium center in **2**. How is the electron transfer event accomplished across three covalent bonds in a kinetically facile fashion and what is the driving force for such a reaction? The proton-coupled electron transfer mechanism, which triggers the disproportionation by inducing very different electrostatic field strengths at the two metal sites, delivers an elegant and intuitively comprehensive solution. Assuming that the mechanism described here is generally applicable for similar dimers, this concept implies a general design requirement. The two metal centers work in concert to concentrate the oxidative power that was delocalized over both centers on one metal site when needed by reforming a Ru(V) center via disproportionation of the Ru(IV)/Ru(IV) intermediate. To facilitate the disproportionation, the bridging ligand must be electronically flexible enough to allow for a smooth electron transfer through the bridge. The spin densities at O1 listed for all intermediates and transition states in Tables 2 and 4 show that the μ-oxo ligand is involved in many electronic communication events that cause notable variations of its spin density. The accumulation of radical character at the μ-oxo unit implies an intrinsic vulnerability of the diruthenium catalyst, as it constitutes a natural center for nonproductive side reactions. The principal driving force for the rate determining step identified above uses the same mechanism of *in situ* generation of radicaloid oxygen to catalyze the most difficult first two oxidation steps. Therefore, similar types of reactions are expected to take place at the bridging ligand, which will inevitably lead to destruction of the catalyst. Suggesting possible mechanisms for these unproductive side reactions and discovering means of suppressing them are future challenges.

Whereas the concept of charge induced disproportionation that we outlined above is intuitive, it is not clear which chemical "trigger" is responsible for this effect. The proton transfer from the Ru2-hydroperoxo ligand to the Ru1-hydroxo group obviously adds a positive charge to the formally anionic hydroxo group to yield a neutral water ligand. At the same time, it transforms the formally anionic hydroperoxo ligand to a

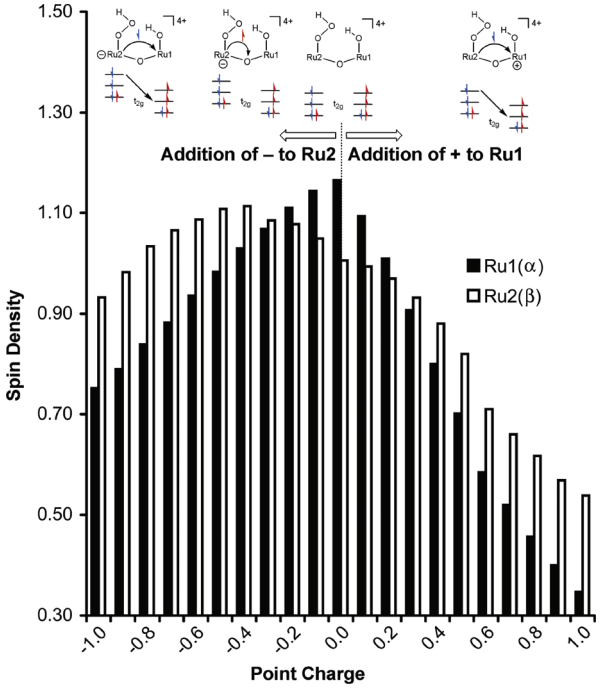

Figure 6. Evolution of Mulliken net spin densities as a function of additional point charge at Ru1 and Ru2, respectively.

dianionic peroxo moiety. Thus, the electrostatic field of Ru2 produced by the ligands becomes significantly stronger, raising the t_{2g}-like frontier orbital energies, whereas the electrostatic field of Ru1 becomes weaker by approximately the same extent. Consequently, the t_{2g}-like frontier orbital energies of Ru1 decrease. Clearly, both effects work in concert to increase the driving force for the intramolecular electron transfer. It is unclear, however, whether the annihilation of the negative ligand charge on Ru1 or the creation of an additional negative charge on Ru2 individually would be capable of promoting the disproportionation. These questions are meaningful because they provide potentially exploitable control features. In the process of rationally designing new catalysts, one can envision gaining control over the disproportionation process by providing a more acidic spectator ligand that would perform the protonation of the hydroxyl ligand. Similarly, engineering a stronger base than the hydroxo group into the catalyst would allow for scavenging the proton from the hydroperoxo group leaving the Ru1−OH fragment untouched.

To answer these questions, we conducted a "theoretical experiment" by placing a point charge q at the coordinates of Ru1 and increasing its charge in increments of 0.1 from zero to one. Analogously, we placed a varying negative charge on Ru2 with the geometry fixed at that of intermediate **2**. The former calculation series simulates the decrease of the electrostatic field strength of the ligands on Ru1, whereas the latter probes for the increase of the electrostatic field on Ru2. Spin densities of Ru1 and Ru2 are plotted against charge $|q|$ in Figure 6. Adding positive charge to Ru1 has the expected effect. The immediate decrease of α-electron density on Ru1 and the decrease of β-electron density at approximately the same extent on Ru2 indicate transfer of β-electron density from Ru2 to Ru1. Adding a negative charge to Ru2, however, has an unexpected response: The β-electron density on Ru2 increases and reaches a maximum at a critical point charge of −0.4 with an electron density of −1.113 compared to the spin density of −1.006 in the unperturbed intermediate **2**. Further increase of negative point charge gives the expected decrease of β-electron density. A detailed inspection of the spin density flux including ligand-based atoms (Supporting Information) shows that Ru2 transfers α-electron density to the bridging oxo moiety at the beginning and promotes the expected β-electron density transfer to Ru1 to a notable extent only when the point charge is increased beyond the critical value of −0.4. The asymmetry of the spin density evolution illustrated in Figure 6 is remarkable. Taken together, these trends identify the weakening of the electrostatic field on Ru1 to be the most efficient promoter for the disproportionation event. Thus, it should in principle be possible to trigger such a reaction by providing an external proton source that may protonate the hydroxyl group independently from the hydroperoxo ligand. Such a reaction may give rise to the production of hydrogen peroxide instead of dioxygen in highly acidic media. The reversed scenario, where a strong external base may deprotonate the hydroperoxo group, is not likely to be an efficient pathway for catalysis.

Comparison with Isotope-Labeling Studies. ^{18}O-Isotope labeling studies provided valuable clues about the mechanism.[2,5,6,20] In these studies, ^{18}O-enriched **[3,3]**$^{4+}$ ion was generated and oxidized to its **[3,4]**$^{4+}$ form that was shown to have negligible water−ligand exchange rates.[48,52] The amount of $^{16}O_2$, $^{16}O^{18}O$, and $^{18}O_2$ produced upon exposure to isotopically dilute solvent was analyzed quantitatively in a time-resolved experiment. No significant production of $^{18}O_2$ was found at any time ruling out intramolecular mechanisms that involve direct coupling of the two terminal oxo groups (C and D in Scheme 1). Interestingly, both $^{16}O_2$ and $^{16}O^{18}O$ were produced at approximately the same rate immediately and consistently.[6] The mechanism discussed above explains the generation of $^{16}O^{18}O$, where one of the oxygen atoms originates from the marked Ru═O moiety and the other is contributed by the solvent water. The immediate production of $^{16}O_2$, however, cannot be explained by the mechanism discussed in this work. Instead, our mechanism predicts a significant time delay for the production of $^{16}O_2$, as the initially marked catalysts must incorporate solvent water during catalysis.

A few mechanistic scenarios can be envisioned for the immediate production of purely solvent derived dioxygen. Figure 7 illustrates two intuitively plausible reactions. Intermediate **5**, the superoxo/aqua-complex could be attacked by an additional water molecule. The superoxo group is particularly interesting for such an attack, as it displays radical character with spin densities of 0.44 and 0.55 on O3 and O4, respectively (Table 4), indicating that there is no obvious bias toward O3 or O4 as the likely attack site. Initial attack at the O3 position yields intermediate **5a**, whereas the reaction at O4 gives **5b**. In principle, the hydrogen trioxide group can rearrange to give an ozonoid intermediate **5c**, as was speculated upon previously.[53] We were able to locate **5a** and **5b** as local minima, but found their electronic energy to be 18.5 and 16.5 kcal/mol higher than intermediate **5** and free water. We estimated the solution phase free energies to be 35.9 and 36.5 kcal/mol uphill for **5a** and **5b** relative to **5**, respectively. Although the transition states were not located, the thermodynamics prohibits any reactive chemistry

(52) Hurst, J. K.; Zhou, J.; Lei, Y. *Inorg. Chem.* **1992**, *31*, 1010−1017.
(53) Meyer, T. J. In *Oxygen Complexes and Oxygen Activation by Transition Metals*; Plenum Press: New York, 1988; pp 33−47.

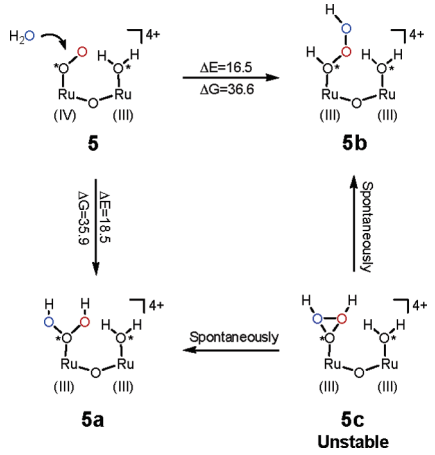

Figure 7. Illustration on the thermodynamic formation of ozonoid intermediate **5a** and hydrotrioxide isomer **5b**. Energies are given in kcal/mol.

involving **5a** or **5b** at reasonable conditions. The kinetic barriers will be notably higher than 36 kcal/mol. The ozonoid species **5c** is not stable, as it relaxes spontaneously to **5a** or **5b**. Although more work is required before a final conclusion can be drawn, it is clear that the concomitant attack of two water molecules cannot be accomplished in a straightforward fashion. We currently have no explanation for the immediate generation of the purely solvent derived dioxygen.

Conclusions

We presented for the first time a complete theoretical treatment of one possible mechanism for the catalytic oxidation of water by *cis,cis*-[(bpy)$_2$Ru^{V}O]$_2$O^{4+}. We considered all plausible spin coupling schemes between the two Ru(V)-d^3 centers and found the AF-coupled high-spin state to be most plausible as the catalytically competent intermediate. The computed rate determining activation barrier of 25.9 kcal/mol is in reasonable agreement with experimental estimates of 18.7−23.3 kcal/mol.[4] Our calculations suggest that the fundamental basis for the catalytic activity lies in a highly spin-polarized Ru^V═O core structure, which formally undergoes an intramolecular electron transfer to give a Ru^{IV}−O• species acting as a strong oxidant that attacks a water molecule to cleave the H−OH bond in a homolytic fashion. Subsequently, proton coupled electron transfer accompanied by ligand charge-controlled intramolecular disproportionation generates a highly electron-deficient Ru(V) center, which completes the overall four-electron redox reaction. We identified a low-energy pathway for the last redox reaction by invoking intersystem crossing to a ferromagnetically coupled intermediate, which gives rise to the generation of a triplet dioxygen.

Whereas our study provides a detailed inside view of the water oxidation mechanism, a number of challenges remain to be addressed in the future. Most importantly, we were unable to explain how purely solvent derived dioxygen can be generated immediately. One possible reaction pathway that involves the concomitant attack of two water molecules to yield an ozonoid intermediate was found to be too high in energy. Furthermore, it is unclear whether the electronic features identified in this study are generally applicable for similar systems. We are currently exploring structural and functional analogues of the diruthenium complex to address this question. Last, we must understand in greater detail why some of the plausible mechanisms are not operative. For example, the concept of in situ generation of the radicaloid oxyl moiety would intuitively suggest that the formation of the "dimer of dimers"[2] should be a favorable process resembling a radical recombination reaction. Our exploratory calculations indicated, however, that there is no notable intermolecular attraction between the terminal oxygen groups. Similarly, it is unclear why the direct intramolecular O−O coupling is not viable. Studies aimed at answering these questions are currently underway in our laboratory.

Acknowledgment. We thank NIH (HG003894) and NSF (0116050) for financial support. We thank the reviewers for very helpful comments.

Supporting Information Available: Complete description of the computational details, additional Mulliken spin density analysis, Cartesian coordinates of all structures and all energy components. This material is available free of charge via the Internet at http://pubs.acs.org.

JA053710J